# TEMPO-Oxidized Cellulose Nanofibrils Reinforce Low-moisture Tobacco Granules through Nanofibrillar Networking and Molecular Immobilization

Songjin Zheng,[a] Yinling Liu,[b] Di Kang,[a] Wei Shen,[a] Yun Zhai,[b] Yuying Fu,[b] and Teng Li,[b,*]

Tobacco granules used as aerosol-generating substrates in heated tobacco products require sufficient mechanical integrity to withstand granulation, handling, screening, and filling, particularly under low-moisture conditions. Low-moisture tobacco granules are prone to weak cohesion because insufficient water limits the mobilization of native binders. Here, TEMPO-oxidized cellulose nanofibrils (TEMPO-CNFs) were incorporated at 1.26 and 2.08% (w/w) to improve their structural integrity. Texture and rheological measurements showed dose-dependent increases in springiness, cohesiveness, apparent viscosity, and storage modulus. Model polyol systems, Fourier transform infrared spectroscopy, and low-field nuclear magnetic resonance indicated that TEMPO-CNFs formed a viscoelastic fibrillar network and reduced the mobility of water, propylene glycol, and glycerol through combined hydrogen-bonding, confinement, and viscosity effects. Thermogravimetric-differential scanning calorimetry revealed essentially unchanged mass-loss stages, maximum mass-loss temperatures (318 to 319 °C), and residues at 400 °C. Thus, TEMPO-CNFs provide a renewable reinforcement strategy for polyol-rich tobacco granules without markedly altering their thermal mass-loss behavior.

*DOI: 10.15376/biores.21.4.11114-11127*

*Keywords: TEMPO Oxidation; Cellulose nanofibrils; Tobacco granules; Rheology; Low-field NMR; Hydrogen bonding*

*Contact information: a: Technology Center, China Tobacco Hebei Industrial Co., Ltd., Shijiazhuang, Hebei 050051, China; b: School of Food Science and Biotechnology, Zhejiang Gongshang University, No. 18 Xuezheng Street, Qiantang District, Hangzhou 310018, China;*
** Corresponding author: tli0718@mail.zjgsu.edu.cn*

## INTRODUCTION

Heated tobacco products generate an inhalable aerosol by heating rather than combusting a tobacco substrate. By avoiding combustion, these products generally produce aerosols containing lower levels of many harmful and potentially harmful constituents than conventional cigarette smoke, although they are not free of toxicants and should not be considered harmless (Bekki *et al.* 2017; Mallock *et al.* 2018). Their consumable units commonly contain reconstituted tobacco sheets or tobacco granules (Gao *et al.* 2014; Huang *et al.* 2024). In such products, tobacco granules serve as part of the aerosol-generating tobacco substrate and must maintain sufficient structural integrity during granulation, conveying, screening, filling, and subsequent handling. Tobacco granules are generally produced by blending finely ground tobacco with aerosol-forming agents, particularly propylene glycol and glycerol, followed by granulation to obtain particles of

approximately 1 to 2 mm. The mechanical integrity of both the moist feed and the resulting granules is important for granulation, conveying, screening, and filling (Luo *et al.* 2021; Wei *et al.* 2023). Excessive moisture may adversely affect processing and product sensory properties; consequently, only a limited amount of water is normally used. Under low-moisture and high-polyol conditions, however, the dissolution and migration of native adhesive components, including soluble carbohydrates, are restricted. Consequently, it is difficult to establish a continuous binding phase between tobacco particles, resulting in poor cohesion, limited elastic recovery, and susceptibility to breakage and powder generation during handling (Wu *et al.* 2019; Zhang *et al.* 2025b). Previous studies have shown that cellulose-fiber refinement and nanocellulose incorporation can improve the strength and structural integrity of reconstituted tobacco matrices (Liu *et al.* 2019; Song *et al.* 2021).

Nanocellulose derived from renewable lignocellulosic resources has attracted considerable interest as a reinforcing material because of its high aspect ratio, large specific surface area, biodegradability, and favorable mechanical properties (Isogai *et al.* 2011). Among the available forms of nanocellulose, TEMPO-mediated oxidation produces cellulose nanofibrils bearing abundant surface carboxylate groups while retaining numerous hydroxyl groups. In the TEMPO/NaBr/NaClO system, the primary hydroxyl groups at the C6 position of cellulose are selectively converted into carboxylate groups (Saito *et al.* 2006, 2007). The resulting electrostatic repulsion promotes fibril individualization and dispersion (Nechyporchuk *et al.* 2016b). The hydroxyl- and carboxylate group-rich surfaces can also interact with water, polyols, and oxygen-containing tobacco components. In addition, the elongated and flexible fibrils can overlap and entangle, thereby providing physical bridges and stress-transfer pathways within particulate formulations (Nechyporchuk *et al.* 2016a; Hubbe *et al.* 2017).

Previous studies on tobacco granules have mainly focused on the effects of tobacco type, aerosol-former composition, and heating conditions on thermal conversion and aerosol release (Wang *et al.* 2019). However, the potential of TEMPO-oxidized cellulose nanofibrils (TEMPO-CNFs) to reinforce low-moisture tobacco granules has received little attention. We hypothesized that TEMPO-CNFs could improve granule cohesion through two complementary mechanisms: the formation of a percolated nanofibrillar network and interfacial association with polyols, water, and tobacco components, thereby reducing molecular mobility. Accordingly, TEMPO-CNFs were prepared and characterized in terms of their morphology, apparent hydrodynamic size, zeta potential, and carboxylate group content. Their effects on the textural and rheological properties of tobacco granules were evaluated. Model-system rheology, Fourier transform infrared spectroscopy (FTIR), and low-field nuclear magnetic resonance (LF-NMR) were used to investigate the underlying interactions, while thermogravimetric–differential scanning calorimetry (TG–DSC) was conducted to determine whether reinforcement with TEMPO-CNFs altered the thermal mass-loss behavior of the granules.

## EXPERIMENTAL

### Materials

An aqueous cellulose nanofibril dispersion with a solids content of 6% was supplied by Shaoxing Yuewei New Materials Technology Co., Ltd. (Shaoxing, China). Sodium bromide, 2,2,6,6-tetramethylpiperidine-1-oxyl (TEMPO), sodium hypochlorite solution

(available chlorine ≥30%), propylene glycol, glycerol, sodium hydroxide and hydrochloric acid were of analytical grade and purchased from Macklin Biochemical Co., Ltd. (Shanghai, China). Flue-cured tobacco screening fragments were provided by China Tobacco Hebei Industrial Co., Ltd. (Shijiazhuang, China), ground and passed through a 200-mesh sieve (75 μm). Deionized water was used throughout the study.

## Preparation of TEMPO-Oxidized Cellulose Nanofibrils

TEMPO-CNFs were prepared by adapting established TEMPO/NaBr/NaClO oxidation protocols (Isogai and Kato 1998; Saito and Isogai 2004). The initial cellulose nanofibril dispersion was diluted to 0.592% (w/w) and stirred until homogeneous. Sodium bromide (11.50 mmol/L), TEMPO (1.22 mmol/L), and sodium hypochlorite (10.00 mmol per gram of dry cellulose nanofibrils) were then added. During oxidation, the pH was maintained at 10.0 ± 0.1 with 0.5 mol/L NaOH under continuous stirring. The reaction was considered complete when no further decrease in pH was observed for 30 min. The suspension was centrifuged at 10,000 rpm for 10 min at room temperature. The collected material was washed twice with deionized water, redispersed, subjected to high-speed shearing at 8,000 rpm for 20 min, and ultrasonicated in an ice bath for 10 min (Saito *et al.* 2007). The resulting TEMPO-CNFs dispersion was stored at 4 °C. Its solids content, determined by drying to constant mass, was 1.95%. A portion of the resulting dispersion was freeze-dried, and the obtained dry TEMPO-CNFs powder was used for the preparation of tobacco granules and for analyses requiring dry material.

## Preparation of Tobacco Granules

Ground tobacco, freeze-dried TEMPO-CNFs powder, propylene glycol, glycerol, and deionized water were used to prepare the tobacco granules. TEMPO-CNFs were incorporated at 0, 1.26, or 2.08% (w/w) of the final formulation, and the corresponding samples were designated TG-control, TG-1.26TC, and TG-2.08TC, respectively. Propylene glycol, glycerol, and water were maintained at 3, 12, and 10% (w/w), respectively, in all formulations, with ground tobacco accounting for the remaining mass. Thus, on a 100-g formulation basis, TG-control contained 75.00 g ground tobacco, 3.00 g propylene glycol, 12.00 g glycerol, and 10.00 g deionized water; TG-1.26TC contained 73.74 g ground tobacco, 1.26 g TEMPO-CNFs powder, 3.00 g propylene glycol, 12.00 g glycerol, and 10.00 g deionized water; and TG-2.08TC contained 72.92 g ground tobacco, 2.08 g TEMPO-CNFs powder, 3.00 g propylene glycol, 12.00 g glycerol, and 10.00 g deionized water. All ingredients were transferred to a grinder and mechanically blended at 800 rpm for 30 min to obtain a homogeneous mixture and ensure uniform distribution of the freeze-dried TEMPO-CNFs powder throughout the tobacco matrix. Each formulation was then processed using a YK-60 oscillating granulator (Shanghai Tianhe Machinery Equipment Co., Ltd., Shanghai, China) to produce granules with an approximate diameter of 1.5 mm. The samples were sealed immediately and stored until analysis.

## Characterization of TEMPO-CNFs

*Atomic force microscopy*

The TEMPO-CNFs dispersion was diluted to 0.01% (w/w), and a 10.0 μL aliquot was deposited on freshly cleaved mica. After drying overnight at room temperature, the samples were imaged in tapping mode using a Dimension Icon atomic force microscope equipped with an OLTESPA-R3 probe (Bruker, Germany). Fibril morphology was analyzed using NanoScope Analysis 3.0 software. The lengths of at least 100 fibrils were

measured to construct a length frequency distribution, and height profiles across individual fibrils were used to estimate fibril thickness (Levanič *et al.* 2020).

*Hydrodynamic size ($D_h$) and ζ-potential*

The TEMPO-CNFs dispersion was diluted to 0.05% (w/w). The apparent Z-average size and zeta potential were measured at 25 °C using a Zetasizer Nano ZS instrument (Malvern Instruments, UK). Because light-scattering measurements report an $D_h$ for anisotropic nanocellulose, the values were interpreted together with the AFM dimensions (Fraschini *et al.* 2014).

*Carboxylate group content*

The surface carboxylate group content was measured by conductometric titration (Li *et al.* 2020). A TEMPO-CNFs dispersion (0.3% (w/w)) was stirred for 10 min and acidified to pH 2.5 with 1.0 mol/L HCl to protonate the carboxylate groups. The acidified dispersion was titrated with standardized 0.03 mol/L NaOH while conductivity was continuously recorded using a DDS-11A conductivity meter (Shanghai Yueping Scientific Instrument Co., Ltd., Shanghai, China). The carboxylate group content was calculated as follows,

$$X = (C \times V / m) \times 10^6 \quad (1)$$

where $X$ is the carboxylate group content (μmol/g), $C$ is the NaOH concentration (mol/L), $V$ is the volume of NaOH consumed in the weak-acid neutralization region (L), and $m$ is the dry mass of TEMPO-CNFs in the titrated dispersion (g).

## Rheological Measurements

Rheological measurements were performed with reference to established protocols for cellulose nanomaterial dispersions (Kumar *et al.* 2016; Nechyporchuk *et al.* 2016a). Measurements were conducted at 25.0 ± 0.1 °C using an MCR 302 rheometer (Anton Paar, Graz, Austria) equipped with a 50-mm parallel-plate geometry and a gap of 1.0 mm. The tested systems included TEMPO-CNFs dispersions at 0.5, 1.0 and 1.5% (w/w); model mixtures containing 1.0% (w/w) TEMPO-CNFs and a propylene glycol/glycerol blend (1:4, w/w) at total polyol contents of 15 or 25% (w/w); and the three tobacco granule formulations. Steady-shear measurements were conducted over 0.01 to 1000 $s^{-1}$, with 10 points collected per decade. Oscillatory strain sweeps were first performed at 1.0 Hz over 0.01 to 1000% strain to establish the linear viscoelastic region. Frequency sweeps were subsequently conducted at 0.5% strain over 1 to 100 Hz, with 25 points per decade, to obtain the storage modulus ($G'$) and loss modulus ($G''$).

## Texture Profile Analysis

Texture profile analysis was used to evaluate the mechanical response of lightly compacted granule masses according to the principle of two-cycle compression testing (Bourne 1978). The prepared granules were gently compacted in a mold to obtain approximately spherical specimens with a diameter of 2 cm. Measurements were performed using a TA.XT.Express texture analyzer fitted with a P36R cylindrical probe (Stable Micro Systems, Surrey, UK). The pre-test, test and post-test speeds were 1, 2 and 2 mm/s, respectively, and the compression strain was 50%. Springiness and cohesiveness were calculated from two successive compression cycles as indicators of elastic recovery and internal binding.

### Fourier Transform Infrared Spectroscopy

Tobacco powder, freeze-dried TEMPO-CNFs, the TEMPO-CNFs/propylene glycol/glycerol model mixture, and TG-2.08TC were dried overnight at 50 °C and compressed into thin specimens (Yuan *et al.* 2019). FTIR spectra were recorded using a Nicolet iS5 spectrometer (Thermo Fisher Scientific, USA) over 400 to 4000 $cm^{-1}$ at a resolution of 4 $cm^{-1}$, with 32 scans accumulated for each spectrum (Geng *et al.* 2018).

### Low-Field Nuclear Magnetic Resonance

The transverse relaxation behavior of the three tobacco granule formulations was measured using a MesoMR23-060H-I LF-NMR analyzer (Niumag Analytical Instrument Corp., Suzhou, China) operating at 0.47 T and a proton resonance frequency of 21 MHz (Bertram *et al.* 2002; Gilbert and Turgeon 2026). A 5.0-g sample was loaded into a cylindrical NMR tube with an internal diameter of 18.0 mm to a height of approximately 2.0 cm. A Carr-Purcell-Meiboom-Gill sequence was applied with a 90° pulse width of 13 μs, an echo spacing of 0.1 ms, 2000 echoes, 16 scans, and a repetition interval of 2 s (Colsenet *et al.* 2005). The decay curves were inverted using the simultaneous iterative reconstruction technique implemented in the instrument software to obtain transverse relaxation-time distributions.

### Thermogravimetric-Differential Scanning Calorimetry

The thermal mass-loss behavior of the three tobacco granule formulations was evaluated using an STA 409 PC simultaneous thermal analyzer (NETZSCH, Germany), following established thermal-analysis procedures for tobacco materials (Dai *et al.* 2021; Zhang *et al.* 2025a). Samples of 8 to 10 mg were placed in alumina crucibles and heated from 30 to 400 °C at 10 °C/min under nitrogen. TG, derivative thermogravimetric (DTG), and DSC signals were recorded to compare mass-loss stages, thermal events, and the temperature corresponding to the maximum mass-loss rate (Wang *et al.* 2019; Gong *et al.* 2023).

### Statistical Analysis

All experiments were performed in triplicate (n = 3), unless otherwise specified, and the results are reported as the mean ± standard deviation. Data were analyzed by one-way analysis of variance using IBM SPSS Statistics 27, followed by Duncan's multiple-range test. Differences were considered significant at $p < 0.05$.

## RESULTS AND DISCUSSION

### Morphology and Surface Characteristics of TEMPO-CNFs

The two- and three-dimensional AFM images showed slender, flexible nanofibrils with axial curvature, local twisting, and extensive overlap (Fig. 1a and b). The observed curvature may reflect disruption of less ordered cellulose regions during oxidation, high-speed shearing, and ultrasonication (Saito *et al.* 2007; Levanič *et al.* 2020). Fibril lengths ranged mainly from 100 to 1000 nm, with the largest population occurring between 200 and 400 nm (Fig. 1c). Height profiles across isolated fibrils gave an apparent thickness of approximately 6 nm (Fig. 1d). These dimensions are within the range commonly reported for individualized TEMPO-oxidized cellulose nanofibrils (Fukuzumi *et al.* 2013; Levanič *et al.* 2020).

The apparent Z-average size was 411.17 ± 18.43 nm (Fig. 1e), which was of the same order of magnitude as the fibril-length distribution obtained by AFM. Because dynamic light scattering assumes an equivalent hydrodynamic sphere, the value represents an apparent size for the anisotropic fibrils (Fukuzumi *et al.* 2013; Fraschini *et al.* 2014). The zeta potential was -49.10 ± 3.17 mV, indicating a strongly anionic surface and favorable electrostatic stabilization in aqueous dispersion. Conductometric titration yielded a carboxylate group density of 1260 ± 15 μmol/g (Fig. 1f) (Li *et al.* 2020). The high negative charge density resulted from selective conversion of C6 primary hydroxyl groups to surface carboxylate group (Saito *et al.* 2007; Isogai *et al.* 2011). Together with the high aspect ratio and abundant hydroxyl groups, these surface characteristics may provide TEMPO-CNFs with the potential to form fibrillar networks and interact with components of the polyol-rich tobacco matrix.

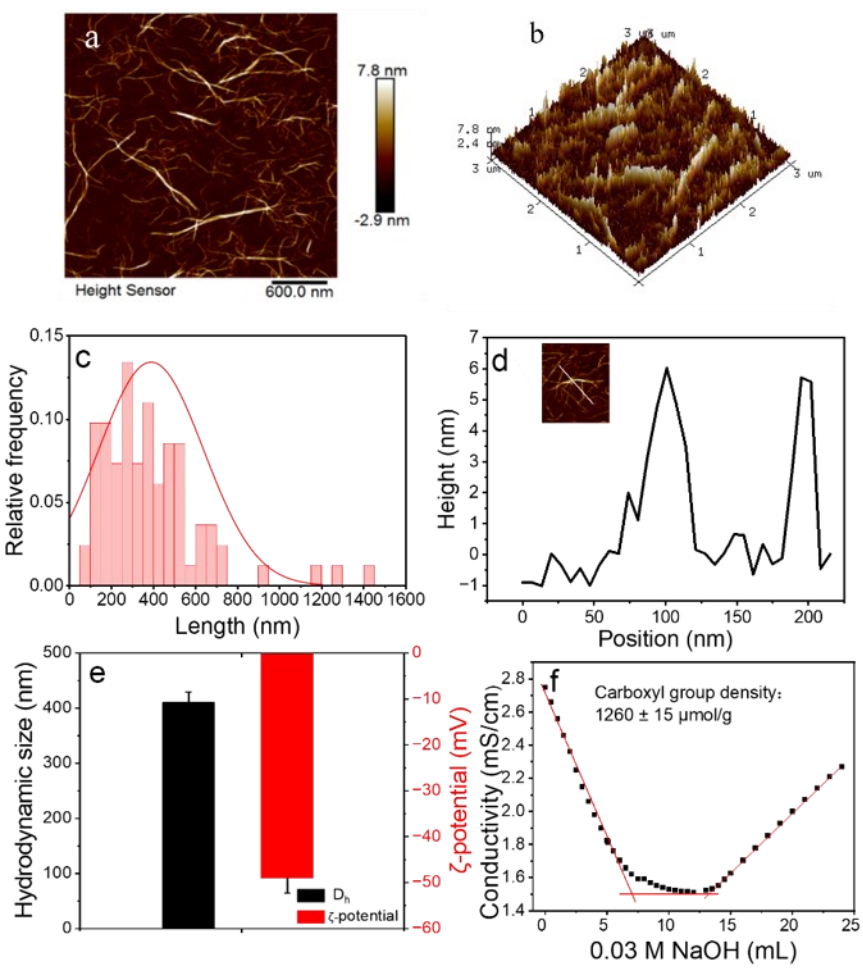



**Fig. 1.** Characterization of TEMPO-oxidized cellulose nanofibrils (TEMPO-CNFs): (a) two-dimensional and (b) three-dimensional AFM images; (c) fibril-length distribution; (d) representative height profile; (e) hydrodynamic size ($D_h$) and *ζ*-potential; and (f) conductometric titration curve and calculated carboxylate group density

## Textural and Rheological Reinforcement of Tobacco Granules

The TG-control exhibited the lowest springiness and cohesiveness among the three formulations (Fig. 2a), consistent with a weakly connected structure and limited recovery after deformation. In this context, higher springiness is favorable because it reflects

improved elastic recovery and reduced permanent deformation during granulation, conveying, screening, and filling. Incorporation of 1.26% TEMPO-CNFs significantly increased both parameters ($p < 0.05$), while TG-2.08TC showed the highest values. The results demonstrate improved elastic recovery and internal cohesion of the bulk granulated material.

All formulations displayed pronounced shear-thinning behavior over 0.01 to 1000 $s^{-1}$ (Fig. 2b), which is characteristic of concentrated cellulose-containing dispersions and particulate systems (Kumar *et al.* 2016; Nechyporchuk *et al.* 2016a). The apparent viscosity increased after TEMPO-CNFs addition and was highest for TG-2.08TC, indicating greater resistance to flow at a given shear rate. During oscillatory frequency sweeps, *G′* remained above *G″* throughout 1 to 100 Hz for all tobacco formulations (Fig. 2c), confirming predominantly elastic behavior (Kumar *et al.* 2016). TEMPO-CNFs-containing samples showed higher *G′* values than the control, and the increase was most pronounced at 2.08%. The concurrent increases in springiness, cohesiveness, apparent viscosity, and *G′* support the formation of a more continuous load-bearing structure after nanofibril incorporation (Hubbe *et al.* 2017).

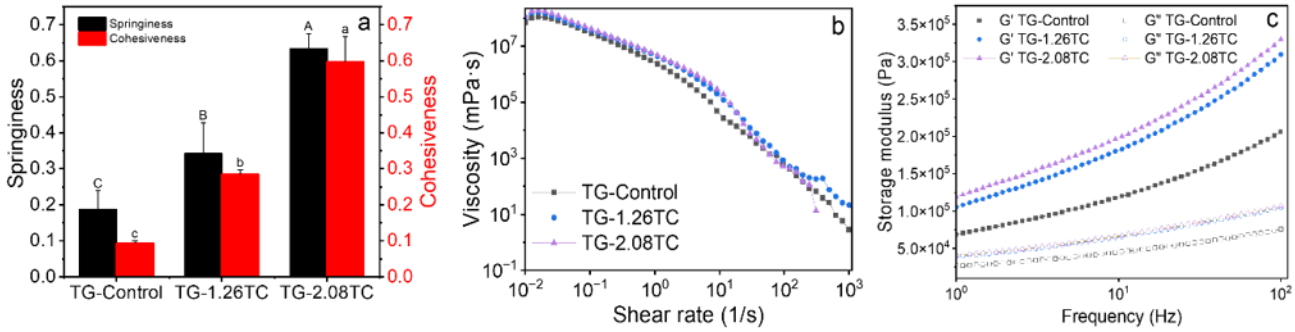



**Fig. 2.** Textural and rheological properties of tobacco granule formulations: (a) springiness and cohesiveness; (b) apparent viscosity as a function of shear rate; and (c) storage modulus (*G′*) and loss modulus (*G″*) as a function of frequency. Different uppercase and lowercase letters indicate significant differences among groups for variables plotted on the left and right y-axes, respectively ($p < 0.05$).

## Viscoelastic Behavior of TEMPO-CNFs/Polyol Model Systems

Frequency sweeps of TEMPO-CNFs dispersions showed that the dynamic moduli increased markedly with fibril concentration (Fig. 3a). At lower frequencies, *G′* exceeded *G″*, indicating that the interconnected fibrils responded as a weak elastic network (Kumar *et al.* 2016; Nechyporchuk *et al.* 2016a). At higher frequencies, *G″* approached or exceeded *G′* in some dispersions, suggesting that the network could not fully reorganize on the shorter deformation timescale. Rather than indicating irreversible bond rupture alone, this crossover reflects the combined effects of fibril relaxation, reversible association, and hydrodynamic interactions (Nechyporchuk *et al.* 2016a).

When the 1.0% (w/w) TEMPO-CNFs dispersion was combined with 15 or 25% (w/w) of the propylene glycol/glycerol blend, *G′* remained above *G″* throughout the tested frequency range (Fig. 3b), and the moduli increased with polyol content. Both polyols contain multiple hydroxyl groups and can interact with cellulose surfaces (Piao *et al.* 2022). Their addition also increases continuous-phase viscosity and reduces fibril mobility, favoring persistent fibril-fibril contacts and a more elastic response (Kumar *et al.* 2016; Zhao *et al.* 2022).

The model system does not reproduce the full complexity of the tobacco matrix, but it demonstrates that TEMPO-CNFs retain the ability to establish a viscoelastic network in the presence of the major aerosol-forming agents used in the granule formulation.

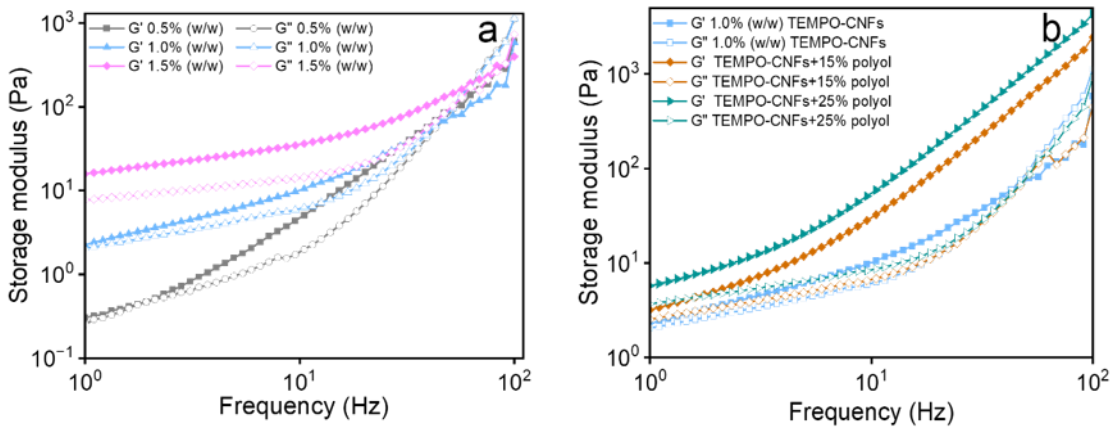



**Fig. 3.** Dynamic rheological behavior of (a) TEMPO-CNFs dispersions at 0.5, 1.0, and 1.5% (w/w) and (b) 1.0% (w/w) TEMPO-CNFs dispersions containing 0, 15, or 25% (w/w) of a propylene glycol/glycerol mixture (1:4, w/w)

## Interactions and Molecular Mobility in Tobacco Granules

The FTIR spectrum of TEMPO-CNFs showed characteristic bands at approximately 1163, 1602, and 3325 $cm^{-1}$ (Fig. 4a). The band near 1163 $cm^{-1}$ was assigned to asymmetric C-O-C stretching in the cellulose backbone, while the band near 1602 $cm^{-1}$ was associated primarily with asymmetric stretching of surface carboxylate groups introduced by TEMPO oxidation (Saito *et al.* 2006, 2007). The broad band centered at 3325 $cm^{-1}$ corresponded to hydrogen-bonded O-H stretching (Yuan *et al.* 2019).

After propylene glycol and glycerol were introduced, the broad O–H stretching band shifted from 3325 to 3302 $cm^{-1}$ and became broader. Because this spectral region contains overlapping contributions from TEMPO-CNFs, propylene glycol, glycerol, residual water, and other hydroxyl-containing components, the shift cannot be assigned to a specific hydrogen-bonding interaction. Rather, the observed red shift and broadening indicate a change in the overall hydrogen-bonding environment of the system, which is consistent with intermolecular association among these components (Yuan *et al.* 2019). The enhanced band around 2930 $cm^{-1}$ mainly reflected the additional aliphatic C-H stretching contributed by the polyols and therefore was not treated as independent evidence of hydrophobic association (Geng *et al.* 2018). For TG-2.08TC, the O–H band shifted further to approximately 3283 $cm^{-1}$, and changes were also observed in the C–O and carboxylate-related regions. Given the chemical complexity of the tobacco matrix and the substantial overlap of vibrational bands, these changes cannot be assigned to a specific molecular interaction. Nevertheless, the overall spectral changes are consistent with alterations in the hydrogen-bonding environment and intermolecular associations among TEMPO-CNFs, polyols, residual water, and oxygen-containing tobacco constituents (Geng *et al.* 2018; Piao *et al.* 2022).

The LF-NMR transverse relaxation distributions contained four distinguishable populations for each formulation (Fig. 4b), indicating proton-containing domains with different mobilities (Colsenet *et al.* 2005). Compared with conventional cut tobacco, the distributions were more complex because the samples contained substantial quantities of both propylene glycol and glycerol in addition to water (Bertram *et al.* 2002; Gilbert and

Turgeon 2026). Because these liquids are mutually miscible and exchange between environments, individual relaxation populations could not be uniquely assigned to a single component.

All major relaxation populations shifted toward shorter $T_2$ values after TEMPO-CNFs addition, and the shift was most evident for TG-2.08TC. Shorter $T_2$ values indicate reduced average proton mobility and stronger interaction with slowly moving or interfacial domains (Colsenet *et al.* 2005; Gilbert and Turgeon 2026). In the present system, the reduction likely arose from a combination of hydrogen bonding, higher macroscopic viscosity, confinement within the fibrillar network, and increased interactions of water and polyol molecules with fibril surfaces (Bertram *et al.* 2002). Thus, LF-NMR does not by itself prove a single type of chemical bond, but, together with the FTIR and rheological results, it demonstrates that TEMPO-CNFs immobilized the water/polyol phase and strengthened coupling between the liquid and solid components of the granules.

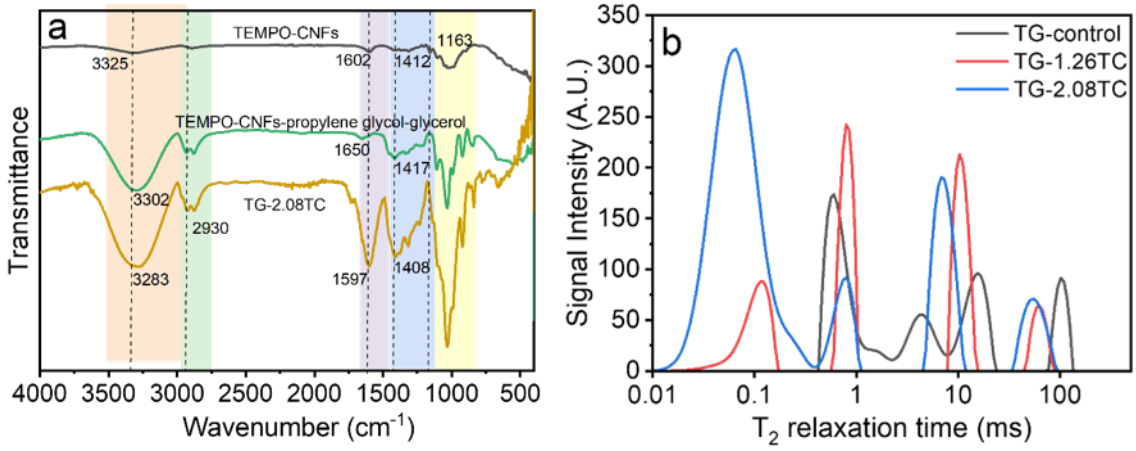



**Fig. 4.** Interactions and molecular mobility in tobacco granule formulations: (a) FTIR spectra of TEMPO-CNFs, the TEMPO-CNFs/propylene glycol/glycerol model mixture, and TG-2.08TC; and (b) LF-NMR transverse relaxation-time distributions of TG-control, TG-1.26TC, and TG-2.08TC

## Thermal Mass-Loss Behavior

The TG, DTG, and DSC profiles of TG-control, TG-1.26TC, and TG-2.08TC were closely similar (Fig. 5). Three broad mass-loss regions were observed between 30 and 400 °C (Dai *et al.* 2021; Zhang *et al.* 2025a). The first region (30 to 140 °C) was mainly associated with water removal and the loss of the most volatile components (Dai *et al.* 2021). The second region (140 to 260 °C) involved volatilization of propylene glycol together with the initial thermal conversion of tobacco polysaccharides and other low-molecular-mass constituents. The third region (260 to 400 °C) included glycerol volatilization and decomposition of cellulose, hemicellulose, and other matrix components (Wang *et al.* 2019; Gong *et al.* 2023).

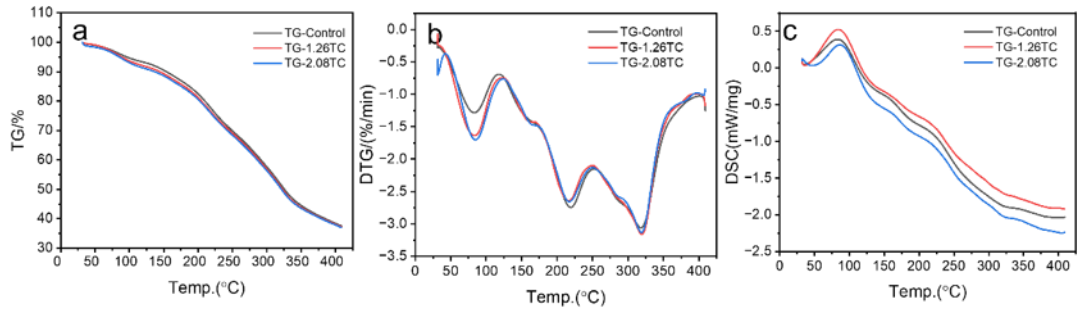



**Fig. 5.** (a) TG (thermogravimetry), (b) DTG (derivative thermogravimetry), and (c) DSC (differential scanning calorimetry) curves of TG-control, TG-1.26TC, and TG-2.08TC under nitrogen

At 400 °C, the residual masses of TG-control, TG-1.26TC, and TG-2.08TC were 38.44, 38.11, and 37.89%, respectively. The main DTG maxima occurred within a narrow range of 318 to 319 °C, and the DSC curves displayed comparable endothermic features associated with volatilization and decomposition (Gong *et al.* 2023). These results indicate that the small amount of TEMPO-CNFs did not markedly change the principal mass-loss stages, peak mass-loss temperature, or final residue under nitrogen.

## Proposed Reinforcement Mechanism

The reinforcement can be interpreted as a multiscale physical process. First, high-aspect-ratio CNFs are known to form interconnected networks through fibril overlap and entanglement in both aqueous and polyol-containing systems (Nechyporchuk *et al.* 2016a; Hubbe *et al.* 2017; Wang *et al.* 2022; Haridevan *et al.* 2022). In the present tobacco-granule system, the increases in $G'$, apparent viscosity, cohesiveness, and springiness after TEMPO-CNFs incorporation are consistent with the formation of a fibrillar network that contributes to structural reinforcement. Second, TEMPO-CNFs have been reported to interact with polyols, including glycerol, and to exhibit distinct network-forming behavior in propylene glycol (Johns *et al.* 2021; Wang *et al.* 2022). In the present system, the FTIR spectral changes, together with the shortened LF-NMR relaxation times, are consistent with association between TEMPO-CNFs and the water/polyol-rich phase and with reduced mobility of the liquid components within the granule matrix.

Previous work has confirmed that heating temperature and glycerol content strongly influence the thermal conversion and aerosol-release behavior of tobacco granules (Wang *et al.* 2019; Dai *et al.* 2021). Conventional binders used in tobacco materials, including methylcellulose, guar gum, pectin, locust bean gum, xanthan gum, and hydroxypropyl methylcellulose, generally reinforce sheet-like products through hydration, thickening, or film formation (Gao *et al.* 2014; Huang *et al.* 2024). TEMPO-CNFs differ in that they provide a high-aspect-ratio physical scaffold in addition to surface interactions. This combination is particularly relevant to a formulation containing limited water and a high proportion of polyols. Importantly, the reinforcement occurred without an appreciable shift in bulk thermal mass-loss behavior, suggesting that the primary effect of TEMPO-CNFs was structural rather than a major modification of the thermal conversion pathways governed by tobacco powder and aerosol-forming agents. Although TEMPO-CNFs showed clear reinforcement potential in low-moisture tobacco granules, practical application in heated tobacco products requires further evaluation of residual TEMPO, its possible transfer into aerosols, and related toxicological risks.

## CONCLUSIONS

1. TEMPO-oxidized cellulose nanofibrils (TEMPO-CNFs) improved the textural and rheological integrity of low-moisture, polyol-rich tobacco granules in a concentration-dependent manner. At 1.26 and 2.08% addition, TEMPO-CNFs increased springiness, cohesiveness, apparent viscosity, and storage modulus.
2. Model-system rheology demonstrated that the fibrils maintained an elastic network in the presence of propylene glycol and glycerol, while Fourier transform infrared (FTIR) and low-field nuclear magnetic resonance (LF-NMR) supported association and reduced molecular mobility in the tobacco formulations.
3. The main thermogravimetric/differential scanning calorimetry (TG-DSC) mass-loss stages, DTG maximum, and residue at 400 °C remained essentially unchanged after TEMPO-CNFs incorporation.
4. The results support a reinforcement mechanism based on nanofibrillar networking, interfacial hydrogen-bonding environments, and physical immobilization of the water/polyol phase. TEMPO-CNFs therefore provide a renewable cellulose-based option for improving granule processability and structural integrity without markedly altering thermal mass-loss behavior.

## ACKNOWLEDGMENTS

This work was supported by the Fundamental Research Funds for the Provincial Universities of Zhejiang (XRK23007) and the University-Enterprise Cooperation Project (1110KH0325016H). The authors thank Dr. Yuewen Chen and Dr. Jie Chen of Zhejiang Gongshang University for assistance with time-domain NMR measurements and texture analysis.

### Conflict of Interest

The authors declare no conflict of interest.

### Use of Generative AI

Generative AI tools were used only for language editing. All scientific content, data interpretation, references, and conclusions were reviewed and verified by the authors.

## REFERENCES CITED

Bekki, K., Inaba, Y., Uchiyama, S., and Kunugita, N. (2017). "Comparison of chemicals in mainstream smoke in heat-not-burn tobacco and combustion cigarettes," *J. UOEH* 39, 201-207. https://doi.org/10.7888/juoeh.39.201

Bertram, H. C., Purslow, P. P., and Andersen, H. J. (2002). "Relationship between meat structure, water mobility, and distribution: A low-field nuclear magnetic resonance study," *J. Agric. Food Chem.* 50, 824-829. https://doi.org/10.1021/jf010738f

Bourne, M. C. (1978). "Texture profile analysis," *Food Technol.* 32, 62-66.

Colsenet, R., Mariette, F., and Cambert, M. (2005). "NMR relaxation and water self-diffusion studies in whey protein solutions and gels," *J. Agric. Food Chem.* 53(17),

6784-6790. https://doi.org/10.1021/jf050162k

Dai, Y., Xu, J., Zhu, L., Jiang, J., Zhou, Y., and Zhou, G. (2021). "Mechanism study on the effect of glycerol addition on tobacco pyrolysis," *J. Anal. Appl. Pyrolysis* 157, article 105183. https://doi.org/10.1016/j.jaap.2021.105183

Fraschini, C., Chauve, G., Le Berre, J.-F., Ellis, S., Méthot, M., O'Connor, B., and Bouchard, J. (2014). "Critical discussion of light scattering and microscopy techniques for CNC particle sizing," *Nord. Pulp Pap. Res. J.* 29, 31-40. https://doi.org/10.3183/NPPRJ-2014-29-01-p031-040

Fukuzumi, H., Saito, T., and Isogai, A. (2013). "Influence of TEMPO-oxidized cellulose nanofibril length on film properties," *Carbohydr. Polym.* 93(1), 172-177. https://doi.org/10.1016/j.carbpol.2012.04.069

Gao, W., Chen, K., Yang, R., and Yang, F. (2014). "Rheological property of reconstituted tobacco coatings," *Ind. Crops Prod.* 60, 45-51. https://doi.org/10.1016/j.indcrop.2014.06.002

Geng, L., Mittal, N., Zhan, C., Ansari, F., Sharma, P. R., Peng, X., Hsiao, B. S., and Söderberg, L. D. (2018). "Understanding the mechanistic behavior of highly charged cellulose nanofibers in aqueous systems," *Macromolecules* 51(4), 1498-1506. https://doi.org/10.1021/acs.macromol.7b02642

Gilbert, A., and Turgeon, S. L. (2026). "Unraveling microstructure and water behavior in diverse food matrices using low-frequency NMR (LF-NMR) on proton: A specific look at 1H-LF-NMR results interpretation," *Food Hydrocoll.* 172, article 111974. https://doi.org/10.1016/j.foodhyd.2025.111974

Gong, X., Zhang, Y., Zhao, W., Duan, Y., Wu, H., Zhang, Z., Jiang, W., Li, X., Han, Y., Ge, Z., *et al.* (2023). "Remarkably enhanced thermal properties of tobacco granules with high-thermal-conductivity nanoparticles," *Heliyon* 9, article e12696. https://doi.org/10.1016/j.heliyon.2022.e12696

Haridevan, H., Chaleat, C., Pooley, L., Evans, D. A. C., Halley, P. J., Martin, D. J., and Annamalai, P. K. (2022). "Processing and rheological properties of polyol/cellulose nanofibre dispersions for polyurethanes," *Polymer* 255, article 125130. https://doi.org/10.1016/j.polymer.2022.125130

Huang, Z., Wang, P., Zhang, J., Zhang, Y., Li, D., Xu, L., Lu, L., Huang, S., Zhou, S., Liu, H., *et al*. (2024). "A facile method to produce high-bulk and high-strength rolled reconstituted tobacco sheet with refined tobacco cellulose fibers," *Cellulose Chem. Technol.* 58(7-8), 771-783. https://doi.org/10.35812/CelluloseChemTechnol.2024.58.70

Hubbe, M. A., Tayeb, P., Joyce, M., Tyagi, P., Kehoe, M., Dimic-Misic, K., and Pal, L. (2017). "Rheology of nanocellulose-rich aqueous suspensions: A review," *BioResources* 12(4), 9556-9661. https://doi.org/10.15376/biores.12.4.Hubbe

Isogai, A., and Kato, Y. (1998). "Preparation of polyuronic acid from cellulose by TEMPO-mediated oxidation," *Cellulose* 5, 153-164. https://doi.org/10.1023/A:1009208603673

Isogai, A., Saito, T., and Fukuzumi, H. (2011). "TEMPO-oxidized cellulose nanofibers," *Nanoscale* 3, 71-85. https://doi.org/10.1039/C0NR00583E

Johns, M. A., Nigmatullin, R., Cranston, E. D., and Eichhorn, S. J. (2021). "The physicochemical effect of sugar alcohol plasticisers on oxidised nanocellulose gels and extruded filaments," *Cellulose* 28, 7829-7843. https://doi.org/10.1007/s10570-021-03991-8

Kumar, V., Nazari, B., Bousfield, D., and Toivakka, M. (2016). "Rheology of

microfibrillated cellulose suspensions in pressure-driven flow," *Appl. Rheol.* 26, article 43534. https://doi.org/10.3933/ApplRheol-26-43534

Levanič, J., Petrovič Šenk, V., Nadrah, P., Poljanšek, I., Oven, P., and Haapala, A. (2020). "Analyzing TEMPO-oxidized cellulose fiber morphology: New insights into optimization of the oxidation process and nanocellulose dispersion quality," *ACS Sustain. Chem. Eng.* 8, 17752-17762. https://doi.org/10.1021/acssuschemeng.0c05989

Li, T., Zhong, Q., Zhao, B., Lenaghan, S., Wang, S., and Wu, T. (2020). "Effect of surface charge density on the ice recrystallization inhibition activity of nanocelluloses," *Carbohydr. Polym.* 234, article 115863. https://doi.org/10.1016/j.carbpol.2020.115863

Liu, H., Liu, Z., Liu, H., Hui, L., Zhang, F., Liu, P., An, X., Wen, Y., and Wu, S. (2019). "Using cationic nanofibrillated cellulose to increase the precipitated calcium carbonate retention and physical properties during reconstituted tobacco sheet preparation," *Ind. Crops Prod.* 130, 592-597. https://doi.org/10.1016/j.indcrop.2019.01.021

Luo, B., An, X., Yang, J., Liu, L., Zhang, H., Hu, Q., Zhang, R., Nie, S., Wu, S., Cao, H., et al. (2021). "Isolation and utilization of tobacco-based cellulose nanofiber (TCNF) for high-performance reconstructed tobacco sheet (RTS)," *Carbohydr. Polym.* 261, article 117865. https://doi.org/10.1016/j.carbpol.2021.117865

Mallock, N., Boss, L., Burk, R., Danziger, M., Welsch, T., Hahn, H., Trieu, H. L., Hahn, J., Pieper, E., Henkler-Stephani, F., Hutzler, C., and Luch, A. (2018). "Levels of selected analytes in the emissions of heat-not-burn tobacco products that are relevant to assess human health risks," *Arch. Toxicol.* 92, 2145-2149. https://doi.org/10.1007/s00204-018-2215-y

Nechyporchuk, O., Belgacem, M. N., and Pignon, F. (2016a). "Current progress in rheology of cellulose nanofibril suspensions," *Biomacromolecules* 17, 2311-2320. https://doi.org/10.1021/acs.biomac.6b00668

Nechyporchuk, O., Belgacem, M. N., and Bras, J. (2016b). "Production of cellulose nanofibrils: A review of recent advances," *Ind. Crops Prod.* 93, 2-25. https://doi.org/10.1016/j.indcrop.2016.02.016

Piao, X., Li, J., Zhao, Y., Guo, L., Zheng, B., Zhou, R., and Ostrikov, K. K. (2022). "Oxidized cellulose nanofibrils-based surimi gel enhancing additives: Interactions, performance and mechanisms," *Food Hydrocoll.* 133, article 107893. https://doi.org/10.1016/j.foodhyd.2022.107893

Saito, T., and Isogai, A. (2004). "TEMPO-mediated oxidation of native cellulose: The effect of oxidation conditions on chemical and crystal structures of the water-insoluble fractions," *Biomacromolecules* 5(5), 1983-1989. https://doi.org/10.1021/bm0497769

Saito, T., Nishiyama, Y., Putaux, J.-L., Vignon, M., and Isogai, A. (2006). "Homogeneous suspensions of individualized microfibrils from TEMPO-catalyzed oxidation of native cellulose," *Biomacromolecules* 7(6), 1687-1691. https://doi.org/10.1021/bm060154s

Saito, T., Kimura, S., Nishiyama, Y., and Isogai, A. (2007). "Cellulose nanofibers prepared by TEMPO-mediated oxidation of native cellulose," *Biomacromolecules* 8(8), 2485-2491. https://doi.org/10.1021/bm0703970

Song, S., Wu, Z., Tan, J., Yang, B., Zhang, M., Lu, P., Wang, J., and Li, W. (2021). "Foam forming: An effective approach to fabricate highly bulky, uniform and soft

reconstituted tobacco sheets," *Cellulose* 28, 2315-2325. https://doi.org/10.1007/s10570-021-03677-1

Wang, C., Li, L., Chen, R., Ma, X., Lu, M., Ma, W., and Peng, H. (2019). "Thermal conversion of tobacco stem into gaseous products," *J. Therm. Anal. Calorim.* 137, 811-823. https://doi.org/10.1007/s10973-019-08010-4

Wang, R., He, H., Sharma, P. R., Tian, J., Söderberg, L. D., Rosén, T., and Hsiao, B. S. (2022). "Unexpected gelation behavior of cellulose nanofibers dispersed in glycols," *Macromolecules* 55, 9527-9536. https://doi.org/10.1021/acs.macromol.2c01035

Wei, P., Li, G., Gao, S., Xiong, B., Tang, X., Tong, Y., Liu, Z., Li, D., Fang, Z., and Yan, Q. (2023). "Effectively reinforcing rolled reconstituted tobacco with carboxymethylated cellulose fibers," *Cellulose* 30, 7129-7140. https://doi.org/10.1007/s10570-023-05318-1

Wu, C., Luo, C., Fan, X., Wang, X., and Wen, Y. (2019). "Evaluation of the potential of tobacco stalk pulp to substitute hardwood pulp for tobacco sheet preparation," *Cellulose Chem. Technol.* 53, 1009-1015. https://doi.org/10.35812/CelluloseChemTechnol.2019.53.99

Yuan, H., Guo, X., Xiao, T., Ma, Q., and Wu, Y. (2019). "Moisture adsorption in TEMPO-oxidized cellulose nanocrystal film at the nanogram level based on micro-FTIR spectroscopy," *Cellulose* 26, 7175-7183. https://doi.org/10.1007/s10570-019-02593-9

Zhang, X., Zhou, S., Zhang, J., Liu, J., Wang, X., Chen, W., Li, Y., Cai, M., Guo, L., and Sun, S. (2025a). "Effects of different heating methods on pyrolysis and smoke release characteristics of tobacco granules," *J. Anal. Appl. Pyrolysis* 189, article 107099. https://doi.org/10.1016/j.jaap.2025.107099

Zhang, X., Gao, J., Zhang, J., Lin, Y., Chen, W., Liu, H., Wang, X., Cao, Y., Tian, H., Zhou, S., and Chen, Q. (2025b). "Understanding the dynamic caking behavior of tobacco granules for heated tobacco products," *Adv. Powder Technol.* 36, 104869. https://doi.org/10.1016/j.apt.2025.104869

Zhao, R., E, S., Ning, D., Ma, Q., Geng, B., and Lu, Z. (2022). "Strengthening and toughening of TEMPO-oxidized cellulose nanofibers/polymers composite films based on hydrogen bonding interactions," *Compos. Commun.* 35, article 101322. https://doi.org/10.1016/j.coco.2022.101322

Article submitted: August 4, 2026; Peer review completed: August 23, 2026; Revised version received: August 26, 2026; Accepted: September 13, 2026, Published: September 28, 2026.
DOI: 10.15376/biores.21.4.11114-11127